Ecohydrologically important subsurface structures in peatlands revealed by ground-penetrating radar and complex conductivity surveys

Nicholas Kettridge,[1] Xavier Comas,[2] Andrew Baird,[3] Lee Slater,[4] Maria Strack,[5] Dan Thompson,[6] Harry Jol,[7] and Andrew Binley[1]

[1] The surface pattern of vegetation influences the composition and humification of peat laid down during the development of a bog, producing a subsurface hydrological structure that is expected to affect both the rate and pattern of water flow. Subsurface peat structures are routinely derived from the inspection of peat cores. However, logistical limits on the number of cores that can be collected means that the horizontal extent of these structures must be inferred. We consider whether subsurface patterns in peat physical properties can be mapped in detail over large areas with ground-penetrating radar (GPR) and complex conductivity by comparing geophysical measurements with peat core data along a 36 m transect through different microhabitats at Caribou Bog, Maine. The geophysical methods show promise. Peat horizons produced radar reflections because of changes in the volumetric moisture content. Although these reflections could not be directly correlated with the peat core data, they were related to the depth-averaged peat properties which varied markedly between the microhabitats. Well-decomposed peat below a hollow was characterized by a discontinuous sequence of chaotic wavy reflections, while distinct layering of the peat below an area of hummocks coincided with a pattern of parallel planar reflections. The complex conductivity survey showed spatial variation in the real and imaginary conductivities which resulted from changes in the pore water conductivity; peat structures may also have influenced the spatial pattern in the complex conductivity. The GPR and complex conductivity surveys enabled the developmental history of the different microhabitats along the studied transect to be inferred.

1. Introduction and Aim of the Research

1.1. Background

[2] Peatlands are prototypical ecohydrological systems. The pattern of vegetation at the peatland surface controls, and is controlled by, hydrological factors. For example, the distribution of different plant species in raised bogs shows a close correspondence with water table position so that "microhabitats" such as hummocks, lawns, hollows, and pools [cf. *Belyea and Clymo*, 1998] have distinctive assemblages of plants and distinctive hydrological regimes. Hummocks tend to contain small-leaved Sphagna and a relatively high cover of sedges and ericaceous shrubs, while lawns and hollows usually contain a lower cover of vascular plants with a high cover of large-leaved Sphagna. However, ecohydrological linkages in peatlands go beyond simple relationships between hydrological regime and the assemblage of plant species.

[3] Different plant communities in peatlands lay down litter or peat of different physical properties which becomes incorporated into the main body of the peat as the peatland grows. These different peats may exert an influence on the ecohydrological functioning of the peatland long after the peat was formed. It has been suggested, for example, that in humid temperate bogs, peat formed in hummocks has a lower permeability than peat formed in hollows because the plant litter that forms the peat in hummocks spends longer above the water table and is therefore more decomposed

[1]Lancaster Environment Centre, Lancaster University, Lancaster, UK.
[2]Department of Geosciences, Florida Atlantic University, Boca Raton, Florida, USA.
[3]Department of Geography, Queen Mary, University of London, London, UK.
[4]Department of Earth and Environmental Sciences, Rutgers University, Newark, New Jersey, USA.
[5]Department of Geography, University of Calgary, Calgary, Alberta, Canada.
[6]School of Geography and Earth Sciences, McMaster University, Hamilton, Ontario, Canada.
[7]Department of Geography and Anthropology, University of Wisconsin-Eau Claire, Eau Claire, Wisconsin, USA.

than the litter in hollows [cf. *Belyea and Baird*, 2006; see also *Boelter*, 1969]. The degree of decomposition of peat will also vary according to the plant species making up the peat, with peat containing vascular plant remains often being more decomposable than that containing *Sphagnum* remains [cf. *Frolking et al.*, 2001; *Moore et al.*, 2007]. If hummocks persist in the peatland landscape, the peat laid down in them may form "columns" of lower-permeability peat. If hummocks coalesce to form ridges, the lower-permeability peat may form curtain-like structures in the peat deposit [*Belyea and Baird*, 2006]. The pattern of lower- and higher-permeability peat in the peat deposit can be expected to affect both rates and patterns of water flow through the peat and, therefore, the spatial pattern of hydrological regimes (e.g., water table regime) across the peatland [*Belyea and Baird*, 2006], which in turn may affect the patterning of vegetation. Such ecohydrological feedbacks have been explored numerically by *Swanson and Grigal* [1988] and *Couwenberg and Joosten* [2005], who used simple cellular models to show that complex patterns of vegetation and of peat transmissivity may emerge from relatively simple interactions between vegetation type and water table position. However, a problem of such studies is that they have not been tested with field data. Although some paleoecological work has shown the spatial continuity of structures within bodies of peat [e.g., *Barber*, 1981], such work relies on the inspection of faces of peat in peatlands that are being cut for peat. Most studies of the subsurface properties of peat use a relatively small number of boreholes (several tens of holes) in which vertical changes in peat type are mapped but from which horizontal variations can only be inferred (if boreholes are constructed along transects).

[4] To test models such as those of *Swanson and Grigal* [1988] and *Couwenberg and Joosten* [2005] and to improve understanding of how subsurface structures within a peat deposit might affect patterns of water flow, it would be very useful if the peat could be mapped noninvasively and in detail over large areas. In theory, information about the level of decomposition of the peat can be obtained using geophysical methods such as ground-penetrating radar (GPR) and complex conductivity.

1.2. Ground-Penetrating Radar

[5] GPR is a geophysical technique for noninvasively identifying changes in the dielectric permittivity between soil layers [e.g., *Huisman et al.*, 2003]. A transmitting antenna generates a high-frequency electromagnetic (EM) wave that penetrates the subsurface and returns to a receiving antenna as a sequence of reflections from the boundaries between materials with contrasting EM properties, such as the boundary between different types of peat or peats with different levels of saturation. The velocity of this EM wave is primarily controlled by the relative dielectric permittivity. Two types of commonly applied GPR reflection surveys are (1) the common offset, where a fixed spacing is maintained between antennae as they are moved stepwise at fixed intervals along a transect, and (2) the common midpoint (CMP) gather, where the antennae are sequentially moved apart at fixed intervals on either side of the measurement position. Common offset measurements are used to construct a transect of the changing physical properties through the ground, recorded as a sequence of reflections in time at each measurement position along the transect. CMP surveys are commonly used to determine the subsurface velocity of the EM wave. With knowledge of the subsurface velocity, the depth of the reflections identified in the common offset measurements can be calculated. In addition, the subsurface velocity can provide a bulk measure of the dielectric permittivity of the peat and can be attributed to changes in peat porosity or saturation [*Comas et al.*, 2008] (see *Jol and Bristow* [2003] and *Neal* [2004] for further details on survey geometry and applications).

[6] GPR has been used for peat deposit profiling for more than 20 years, proving very useful for characterizing the overall depth of peat deposits and the suborganic lithology [*Worsfold et al.*, 1986; *Jol and Smith*, 1991; *Nobes and Warner*, 1991; *Lapen et al.*, 1996]. The boundary between the peat and the underlying mineral sediment is clearly identifiable because of the strong EM wave reflection resulting from the sharp reduction in the volumetric moisture content between the peat and the underlying mineral soil [e.g., *Comas et al.*, 2004]. This strong EM reflection enables the peat depth to be mapped at a high spatial resolution [*Worsfold et al.*, 1986]. However, the stratigraphic information on the peat profile that can be obtained from GPR measurements is less clear. Radar reflection profiles within peat often show a pattern of reflections [cf. *Comas et al.*, 2004]. *Theimer et al.* [1994] suggested that these reflections strongly match variations in peat moisture content (although no radar profiles were presented). However, *Warner et al.* [1990] could only identify the boundary between uppermost poorly decomposed peat ("acrotelm") and underlying well-decomposed peat ("catotelm") [cf. *Ingram*, 1978], and *Worsfold et al.* [1986] suggested a lack of correlation between peat properties and radar reflections.

[7] Although the identification of the boundaries between individual peat horizons from GPR measurements may prove problematic, the potential of GPR to identify the developmental history of different parts of a peatland has not been evaluated. For example, the reflection profile of an area of peatland that has shown numerous switches between different microhabitats may contrast clearly with the reflection profile of a microhabitat that has persisted over the development of the bog. Therefore, instead of attempting to produce direct correlations between the location of peat horizons and EM reflections [e.g., *Worsfold et al.*, 1986], GPR may be applied to identify different "developmental zones" of peat.

1.3. Complex Conductivity

[8] The complex conductivity, σ^*, of a material is composed of the in-phase (real) conductivity, σ', and out-of-phase (imaginary) conductivity, σ'':

$$\sigma^* = \sigma' + i\sigma'', \tag{1}$$

where $i = \sqrt{-1}$. The real conductivity is a measure of how strongly a material supports the flow of electrical current, and the imaginary conductivity is a measure of the polarization, the storage of electrical charge.

1.3.1. Real Conductivity

[9] Below the water table, the real conductivity of peat depends on the pore fluid conductivity, the biogenic gas content (i.e., degree of saturation), and the physical prop-

erties of the peat matrix (porosity and surface area) [*Theimer et al.*, 1994; *Comas and Slater*, 2004; *Slater et al.*, 2007]. The commonly applied parallel electrolytic and surface conduction model may be used for defining the relationship between these properties [e.g., *Comas and Slater*, 2004] for peat soils:

$$\sigma' = \theta_{\mathrm{eff}}^{m} S^{n} \sigma_w + \sigma_{\mathrm{surf}}, \tag{2}$$

where θ_{eff} is the effective porosity, S is the saturation, σ_w is the pore fluid conductivity, σ_{surf} is the surface conductivity (conduction within the electrical double layer that forms at the solid-fluid interface), n is the saturation exponent, and m is the "cementation" factor, which depends on the shape of the pores and their interconnectedness. The first term on the right side of equation (2), Archie's law [*Archie*, 1942], accounts for the electrolytic current flow through the pore water. Although Archie's law has been parameterized for numerous geological materials, few attempts have been made to parameterize the equation for organic soils. *Slater et al.* [2007] suggest that a value for the saturation exponent of ≈1.3 is appropriate for poorly decomposed *Sphagnum* peat. However, they emphasize the approximate nature of this value, with the need for future laboratory experiments to constrain it further.

[10] *Comas and Slater* [2004] show that the first term on the right side of equation (2) must be adapted to simulate the electrical properties of peat under varying pore water conductivities. Their adapted equation accounts for the dilation of the pore space resulting from the flocculation of humic acids located on the surface of the peat fibers. They also suggest that the surface conduction component (σ_{surf}; equation (2)) can be approximated by its linear dependence on the imaginary conductivity, σ'' (section 1.3.2). The adapted version of equation (2), with the exclusion of $\theta_{\mathrm{eff}}^{m}$ and S^{n}, is

$$\sigma' = \sigma_{\mathrm{el}} + \sigma_{\mathrm{surf}} = A\sigma_w^b + C\sigma''(\sigma_w), \tag{3}$$

where σ_{el} is the electrolytic conduction and A, b, and C are constants. *Comas and Slater* [2004] found that A equaled 1.29, b equaled 1.42, and C equaled 63 for a peat sample collected at a depth of $1.0-1.25$ m at Caribou Bog, Maine, USA. Although this model accurately simulates σ' of *Comas and Slater*'s [2004] calibration samples, the model has not been widely evaluated and thus should only be applied with some caution. For example, the model failed to simulate conductivity measurements obtained by *Slater et al.* [2007], possibly because the peat type looked at differed substantially from the peat types studied by *Comas and Slater* [2004].

1.3.2. Imaginary Conductivity

[11] The σ'' is a measure of the storage of charge in the electrical double layer that forms at the solid-fluid interface. Unlike σ', which aggregates the electrolytic and surface conduction into a single measure of conductivity (equation (2)), σ'' is a function solely of the interfacial surface. The σ'' therefore offers an additional, more distinct, measure of the structural attributes of a material than σ' and may improve the distinction between different peat types. Although the dependence of σ'' on the structural attributes of different

peat soils has not been examined, the dependence of σ'' on the surface area per unit pore volume [*Börner and Schön*, 1991; *Börner et al.*, 1996; *Slater and Glaser*, 2003] or the effective grain size [*Vanhala*, 1997; *Slater and Lesmes*, 2002] has been well established within mineral soils, and the approach has been applied within field investigations to differentiate between lithologies not distinguishable with σ' [see, e.g., *Slater and Lesmes*, 2002]. However, σ'' is also a function of the surface charge density and surface ionic mobility within the interfacial boundary [*Lesmes and Morgan*, 2001], with their associated dependence on the pore fluid composition and concentration [*Slater and Lesmes*, 2002]. Whereas the dependence of σ'' on σ_w is minimal for inorganic soils and sandstone [*Lesmes and Frye*, 2001], a power law dependence of σ'' on σ_w with an exponent ≈0.5 was identified for peat soils obtained from Caribou Bog, Maine [*Comas and Slater*, 2004]. Therefore, changes in σ'' cannot be attributed solely to structural variations, such as the surface area per unit pore volume, in peat soils.
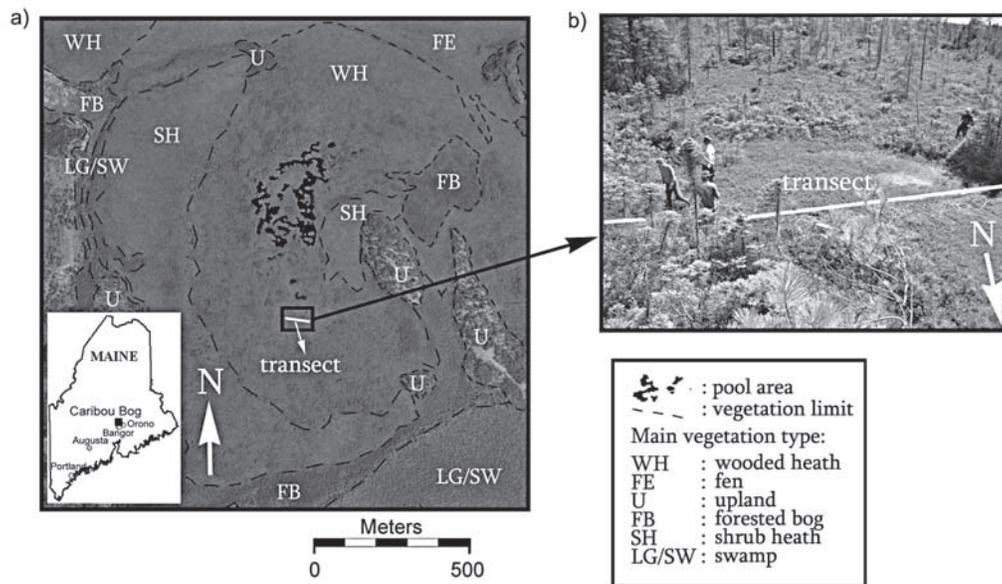
1.3.3. Complex Conductivity Surveys

[12] An electrical survey reconstructs the 2-D or 3-D complex conductivity distribution of the subsurface from a large number of four-electrode resistance measurements (resistance being the reciprocal of conductance). Two electrodes are used to produce an electrical circuit through the peat, and a further two electrodes are used to measure the potential difference that results from the current injection. Complex conductivity surveys performed in the frequency domain inject an alternating current between the electrodes and measure the phase-shifted voltage relative to this injected current. Measured currents and voltages are subsequently converted to an apparent complex electrical conductivity by means of the "geometric factor" that accounts for the spatial arrangement of the four electrodes. This apparent complex conductivity is represented by the conductivity magnitude, $|\sigma|$, and phase angle, ϕ (shift between the injected current and measured potential):

$$\sigma' = |\sigma| \cos\phi, \tag{4}$$

$$\sigma'' = |\sigma| \sin\phi. \tag{5}$$

The subsurface conductivity distribution is calculated by finding the parameterization of a model of subsurface complex conductivity that produces the best predictions of the measured apparent complex conductivities. This process of model parameterization is called inverse modeling.

[13] Surveys performed in the time domain measure the polarization of the ground by abruptly stopping the injection of current and measuring the subsequent decay in the potential with time. The decay curve is integrated between two points to provide a measure of polarization, the chargeability, which is dependent upon the measurement settings of the time domain instrument. To allow inverse modeling ("inversion") of the complex conductivity, measured chargeabilities can be converted into the frequency domain by assuming proportionality between the chargeability and phase angle. Proportionality between chargeability and phase angles is both theoretically and experimentally well established [e.g., *Lesmes and Frye*, 2001; *Slater and Lesmes*, 2002], and the approach has been successfully

Figure 1. Location of Caribou Bog and the study site.

applied to invert 2-D time domain data sets using complex conductivity inversions [*Slater and Binley*, 2003, 2006]. In comparison to the frequency method [see *Binley and Kemna*, 2005], the approach produces scaled images of σ'', the proportionality constant being dependent on the measurement settings of the time domain instrument. The images thus obtained from the complex conductivity inversion faithfully record the relative changes in phase and σ'' within the subsurface (for details see *Slater and Binley* [2003]).

[14] Low-resolution conductivity surveys (electrode spacing 1.5–5 m) have been used to analyze the large-scale stratigraphy of northern peatlands, notably, the identification of the boundary between the peat and the underling mineral sediment and suborganic soil lithology [*Slater and Reeve*, 2002; *Comas et al.*, 2004]. These surveys suggest that σ' is horizontally uniform and may increase with depth through the peat and that the σ'' of the peat remains constant in all spatial directions. However, spatial variations in the peat properties will occur at a scale far smaller than that which can be resolved from these large-scale measurements, including at the scale of the different microhabitats discussed in section 1.1 (10^0–10^1 m). These small-scale spatial variations in electrical properties of the peat will be averaged by large-scale complex conductivity surveys. Variations in the real and imaginary conductivities associated with changing peat structures across microhabitats have therefore not previously been examined.

1.4. Aim

[15] Peat properties may show important variations in the level of decomposition between different microhabitats. As postulated in section 1.1, the resultant spatial variations in peat permeabilities can be expected to affect the spatial pattern of hydrological regimes, which in turn may affect the patterning of vegetation. The aim of this study was to test whether changes in the dielectric permittivity, identified from ground-penetrating radar, or the real and imaginary conductivities, identified from a complex conductivity sur-

vey, could identify differences in the physical properties of peat formed under different microhabitats. If the methods are successful in this respect, they will prove of enormous value in future studies of the ecohydrological functioning of peatlands, as noted at the end of section 1.1.

2. Experimental Design and Methods

2.1. Study Site

[16] The experimental work was carried out at Caribou Bog, a 2200 ha peatland situated near Bangor, Maine, USA (inset in Figure 1a). The study area was part of the largest of three units that comprise the bog, the central unit. This unit, which covers approximately 3.6 km^2, has a topography and stratigraphy characteristic of an eccentric bog [*Davis and Anderson*, 2001], with peat thicknesses reaching 12 m in places, and is characterized by sharp changes in vegetation patterns and the presence of open pools [*Comas et al.*, 2005]. The area chosen for study comprised a wet *Sphagnum* lawn and hollow surrounded by drier microhabitats (Figure 1b). A 36 m transect (Figure 1) was constructed so that it passed through the center of the lawn and hollow. The first 16 m of the transect was in a relatively dry microhabitat dominated by small hummocks with a high cover of shrubs (Table 1). The next 12 m was through the lawn and hollow with a high cover of *Sphagnum* mosses and a general lack of shrubs, with the last 8 m in another relatively dry area dominated by a spruce-tamarack thicket (Table 1). The site was chosen because of the contrasting habitats; it was thought that if the habitats had differences in their developmental histories [*Belyea and Clymo*, 2001], there might be a clear contrast between the properties of the peats formed under them, making the site suitable for testing how well the different geophysical methods could detect differences in peat type.

2.2. Ground-Penetrating Radar Survey

[17] GPR measurements were collected using a Sensors and Software pulseEKKO system, with each measurement

Table 1. Vegetation Along the Transect, Where the Data Represent Percentage Cover[a]

| | Distance (m) | | | | | | | | | | | | | | | | | |
---	0–2	2–4	4–6	6–8	8–10	10–12	12–14	14–16	16–18	18–20	20–22	22–24	24–25	25–27	27–29	29–31	31–33	33–36
Vascular plants																		
Carex sp.									<1	<1	<1	<1	path					
Chamaedaphne calyculata	<1	3	2	7	1	3	5	9	10	10	20	30	path	4	1			7
Drosera rotundifolia	<1	<1							<1	<1			path	<1				
Eriophorum vaginatum	<1	<1	<1	1		3							path	<1				
Kalmia angustifolia	20	10	20	15	15	20	15	4					path	<1	5	8	8	10
Kalmia polifolia	<1	<1	<1					<1	<1	<1	<1		path	<1	<1	<1	<1	
Larix laricina		<1	<1					2					path		8	20	20	15
Ledum groenlandicum	1	2	2	1	<1	3	2	2			<1	<1	path	<1	1	3	3	5
Picea mariana	2	2	8	3	4	8	30	30			<1		path	25	20	45	45	50
Rhododendron canadense													path	<1	<1	<1	<1	
Rhynchospora alba									<1	1	1	<1	path	<1				
Sarracenia purpurea													path	<1				
Vaccinium angustifolium	1	4	6	5	2	3	10	1				<1	path	15	15	15	15	10
Vaccinium oxycoccus	<1	<1						<1	<1	1	<1	<1	path	<1	<1	<1	<1	
Mosses and liverworts																		
Mylia anomala			<1										path			2	2	1
Polytrichum strictum	<1	<1	<1	<1	<1	<1	<1						path					
Sphagnum section cuspidata									65	25			path					
Sphagnum fuscum	30	25	50	35	35	40	35	5					path	1	30	35	35	30
Sphagnum magellanicum	<1	<1	<1	<1	<1	1	<1	20	<1	2	2	<1	path	4	<1			7
Sphagnum rubellum	10	30	30	8	20	5	20	50	30	75	95	100	path	40	15	15	15	15
Lichens	40	25	10	35	35	35	20											

[a]For ease of presentation, data have been presented in 2 m blocks, although some boundaries in the field cut across these blocks (see Figure 1). Cover was estimated to the nearest 1% if under 10% and to the nearest 5% if over 10%. Here <1 denotes that a species was present but with less than 1% cover. Species names follow the nomenclature of *Anderson and Crum* [1981] and *Scoggan* [1978].

stacked 16 times to increase the signal-to-noise ratio. Common offset measurements were collected with 200 MHz antennae, with an antenna separation of 0.5 m, at intervals of 0.1 m along the transect. This frequency provided a high measurement resolution while maintaining strong signal strength through the studied peat profile. Minimal processing was applied to the resultant GPR data. A time-varying gain equalized the amplitude of reflections with depth, accounting for the attenuation of the EM wave. A "dewow" filter removed low-frequency noise and a time zero static correction was applied to correct for drift in the position of the time zero between traces [*Sensors and Software*, 1998; *Jol and Bristow*, 2003].

[18] CMP gathers were collected with 100 MHz antennae at 8, 17, and 25 m along the transect (CMP_1, CMP_2, and CMP_3, respectively). The 100 MHz antenna provided the necessary measurement depth to identify the peat-mineral interface (at a depth of approximately 9–10 m), used as the horizontal reflector to calculate the velocity, v, of the EM wave (Figure 2). The choice of the location of the CMP gathers was based on the distribution of wetter lawn and hollow areas (CMP_2 in Figure 3a) and the surrounding drier microhabitats (CMP_1 and CMP_3 in Figure 3a). The average v of the peat column from surface to mineral soil was obtained by fitting the first arrivals of the reflected wavelet corresponding to the mineral soil reflector with the normal moveout hyperbola (or difference between travel time of the EM wave between transmitter and receiver at a given antenna separation) using a least squares routine [*Neal*, 2004].

2.3. Complex Conductivity Survey

[19] Electrical measurements were made using an array of 72 stainless steel electrodes spaced 0.5 m apart along the transect. Each electrode was inserted through the surface vegetation to a depth sufficient to ensure good electrical contact with the main body of peat (tests showed that the
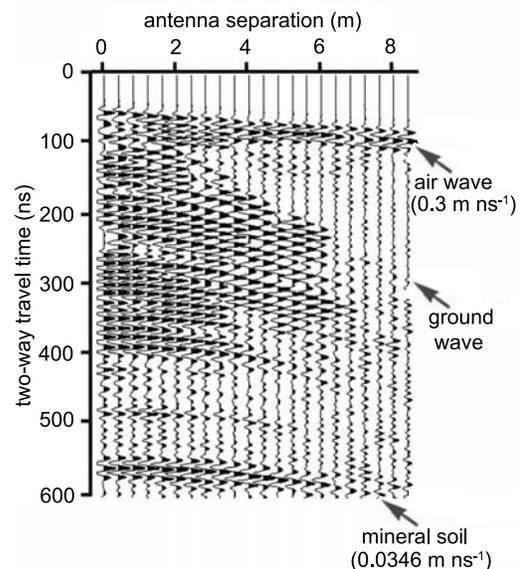
Figure 2. CMP data taken at CMP_2 (Figure 3).
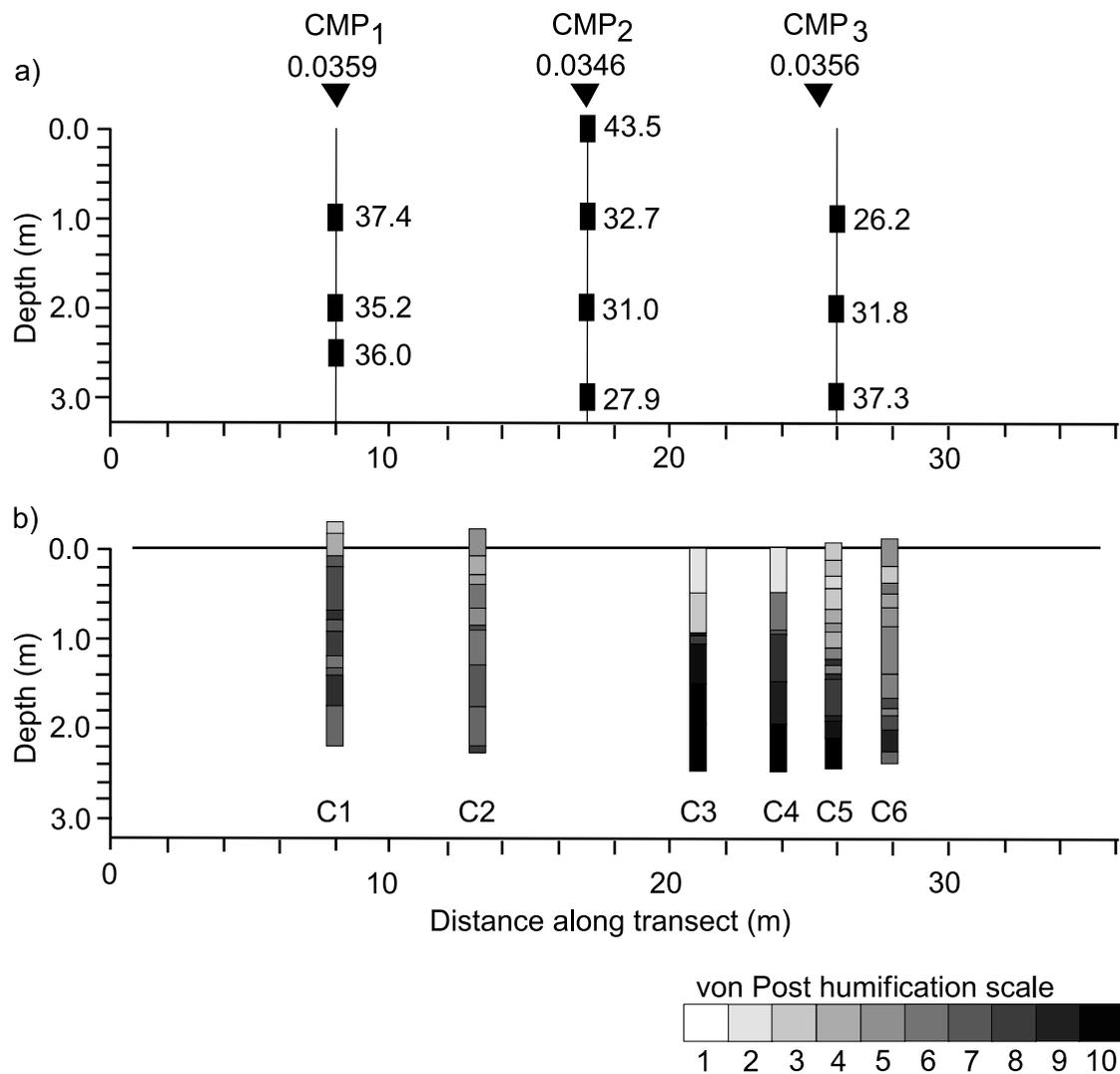
Figure 3. (a) CMP and pore water conductivity measurement locations. EM velocities presented above each measurement location, in m ns^{-1}, and pore water conductivities presented, in μS cm^{-1}. (b) The von Post classification of the peat from the six cores.

contact resistance was less than 6 kΩ between any electrode pair). Data were acquired using a Syscal Pro instrument. The complex conductivity survey was performed in the time domain, and measured chargeabilities were converted to the frequency domain to allow inversion of the complex conductivity (section 1.3.3). A total of 1039 independent measurements were collected using a combination of four-electrode configurations that provided a uniform sampling of the top ~3 m of the peat along the length of the transect. The choice of electrode configuration (i.e., geometrical arrangement of the current injection pair and voltage measurement pair) can exert a strong influence on the reconstructed conductivity image. The electrode configuration affects the spatial sensitivity of the reconstructed image (i.e., how the conductivity distribution of the subsurface image changes in response to the measured resistances) and signal-to-noise ratio. We used a configuration that ensures large voltages (often by straddling the current injection pair), which is critical to collecting reliable chargeability measurements. The measurement quality was evaluated by collect-

ing a complete set of reciprocal data (i.e., an additional 1039 measurements), whereby the voltage and current electrode pairs were interchanged (in theory, these measurements should be identical, and the deviation is a robust measure of the data quality [*LaBrecque et al.*, 1996]).

[20] The three-dimensional current field was simulated using a finite element (FE) model. The model assumed a two-dimensional conductivity structure along the length of the transect. This conductivity structure of the transect was parameterized by minimizing an objective function combining two terms: (1) the least squares, the weighted difference between observed and predicted measurements; and (2) a measure of solution complexity based on a second derivative spatial filter. The two terms were weighted to achieve consistency between simulated and observed measurement errors, i.e., an Occam's inversion [*Constable et al.*, 1987]. To perform the inversion, we utilized a complex conductivity algorithm called CR2 (available from Andrew Binley, Lancaster University) outlined by *Kemna et al.* [2004] and *Binley and Kemna* [2005]. The sensitivity of

the resulting complex conductivity image is depth-dependent. Changes in the subsurface properties close to the ground surface (near to the electrodes) have a larger effect on the measured resistances than a similar change in subsurface properties at depth. This reduced sensitivity produces an increased smoothing of the complex conductivity image with depth that should be borne in mind in the subsequent data analysis.

2.4. Ground Truthing: Topography, Stratigraphic Survey and Specific Conductivity

[21] Microtopographical (10^{-2}–10^0 m) variations of the peatland surface along the transect line were measured using a laser level and were expressed relative to an arbitrary datum. Vegetation was mapped along a 3 m wide band centered on the transect; that is, the vegetation 1.5 m on either side of the transect line was characterized. All plant species within this area were identified, and the surface cover of each was visually estimated using quadrats. Vascular plants were named according to *Scoggan* [1978], while the nomenclature of mosses followed *Anderson and Crum* [1981].

[22] To help interpret the data from the GPR and electrical surveys, six cores of peat were extracted using a Russian corer at distances of 8, 13, 21, 24, 25.8, and 28 m along the transect line, each to a depth of 2.5 m (C1–C6 in Figure 3b). The peat from each core was classified using the von Post scale [*von Post and Granlund*, 1926]. The von Post scale involves in-the-hand assessment of the degree of humification of peat and requires the classification of the peat into 1 of 10 categories, with 1 representing fresh litter and 10 representing intensely humified or decomposed peat in which visible plant remains and structures are absent. Where appropriate, note was also taken of visible plant remains such as woody inclusions or whether the peat was dominated by *Sphagnum* remains or sedges.

[23] Following the same criteria used for the CMP measurements, the specific conductivity of pore water was measured at distances of 8, 17, and 25 m along the transect line as shown in Figure 3a. Pore water was sampled from temporary piezometers with screens 10 cm long inserted at each location and using a hand-operated pump, extracting 16 cm^3 of pore water per stroke. Three to four specific conductivity measurements with depth (surface, 1, 2, and 3 m depth) were acquired using a Hach sensION5 conductivity meter to investigate changes in fluid conductivity that could potentially influence the complex conductivity. Because σ' is directly dependent on σ_w (equation (2)), electrical measurements must account for any significant changes in σ_w.

3. Results

3.1. Vegetation and Stratigraphic Data

[24] The results from the vegetation survey are shown in Figure 4a and Table 1. As noted in section 2.1, there were three broad areas along the transect in terms of vegetation cover. The first 13 m of the transect was dominated by small hummocks (diameters of <1 m), formed mostly of *Sphagnum fuscum* and *S. rubellum*. There was a high cover of shrubs in this area, notably *Kalmia angustifolia*, and a scattering of short (<5 m) trees, almost all black spruce (*Picea mariana*). Bordering the hummock area and the lawn

and hollow (i.e., between 13 and 16 m) was a small spruce thicket, after which there was an open area dominated by *Sphagnum*. The hollow contained Sphagna of the section cuspidata, while the surrounding lawn was dominated by *S. rubellum*. The *S. rubellum* lawn gave way gradually to a low-spreading hummock from about 21 m, which itself gave way rather abruptly at 28 m to a spruce-tamarack thicket (*Picea mariana–Larix laricina*) for the remainder of the transect (to 36 m). The thicket contained some *Kalmia angustifolia* and a relatively high cover of *Sphagnum fuscum* and *S. rubellum* (Table 1).

[25] The core data (Figure 3b) showed a clear correspondence with the vegetation in that there were distinct differences in the layering and degree of humification of the peat between the drier microhabitats and the lawn and hollow. The core taken in the lawn and hollow at 21 m had an upper layer of 0.5 m of poorly decomposed *Sphagnum* remains, in which individual *Sphagnum* plants could still be seen, which was underlain to a depth of 0.95 m by slightly more decomposed peat containing abundant *Sphagnum* and sedge remains. There was then a sharp transition (<1 cm) to a gelatinous peat that was largely amorphous with a high degree of humification. No layering was evident in this lower 1.55 m. A similar profile was evident in the core taken in the low-spreading hummock at 24 m. However, with this core the poorly decomposed peat containing visible *Sphagnum* remains was confined to the upper 0.5 m; this was underlain by a watery layer between 0.5 and 0.95 m containing dark colloidal material that then gave way abruptly to amorphous, gelatinous, highly humified peat.

[26] C1 and C2 in the hummocky area and C6 in the spruce-tamarack thicket were strikingly different from C3 and C4, with a more complicated pattern of layering and more variety in degrees of humification of the different layers (Figure 3). For example, there were at least 10 distinct layers of peat in C1 and C2. This layering probably reveals switches in near-surface wetness and vegetation type when the peat was being formed. For example, between depths of 0.87 and 1.5 m in C2 there is a change from moderately humified peat to strongly humified peat to moderately humified peat again (from von Post scores of 5 between 0.87 and 1.07 m to 7–8 between 1.07 and 1.14 m and to 6 between 1.14 and 1.5 m). These switches may indicate autogenic changes in microhabitat disposition and extent at the peatland surface or they may indicate external forcing, with the less-humified peat forming during wetter and cooler climatic conditions than the more humified peat. Although C6 showed a similar level of complexity in terms of its number and pattern of layers, its layers do not appear to correspond to those of C1 and C2. Correlation between the cores would require absolute dating of different layers, but the evidence suggests that wet and dry episodes at the different locations were, in part at least, independent of each other.

3.2. Ground-Penetrating Radar Results

[27] The peat-mineral interface was clearly identifiable within the CMP gathers (Figure 2), enabling accurate determination of the first arrivals of the reflected wavelets and therefore the accurate calculation of the EM wave velocities. The EM wave velocity shows only a small
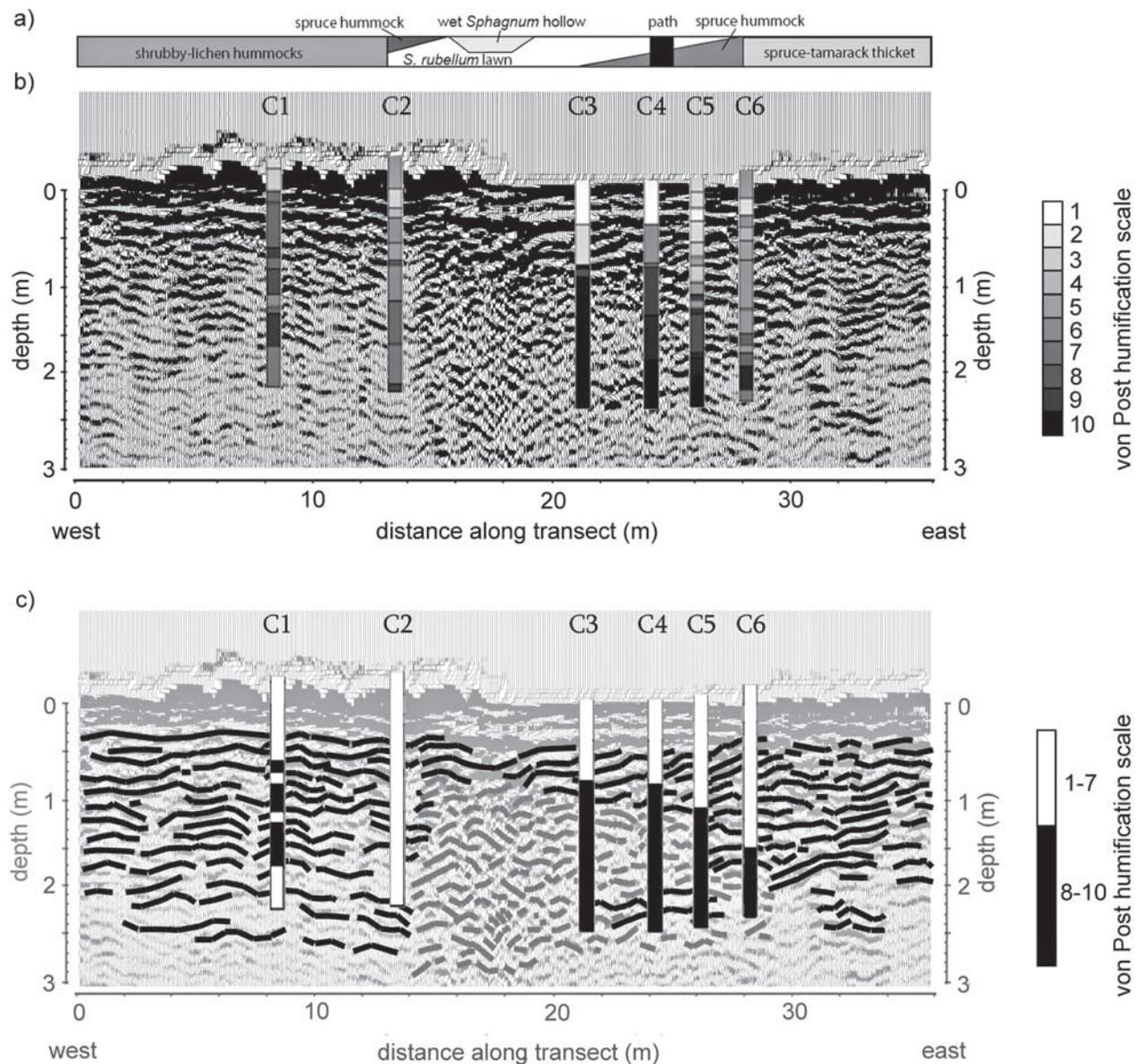
Figure 4. (a) Vegetation types along the west to east study transect. (b) Radar reflection profile from common offset data acquisition. (c) Radar stratigraphic interpretation showing the dominant reflections beneath the ground wave, superimposed upon the radar reflection profile. Reflections are classified into a zone of continuous reflections to semireflections and a zone of chaotic reflections, marked by black and light gray horizontal bands, respectively. Figures 4b and 4c also include the von Post classification of the peat from the six cores.

variation between the different microhabitats (Figure 3a). Drier microhabitats (CMP_1 and CMP_3 corresponding to shrubby-lichen hummocks and a spruce-tamarack thicket, respectively) show v values (plus or minus standard error of the hyperbola regression) of 0.0359 ± 0.00044 and 0.0356 ± 0.00021 m ns^{-1}, respectively, and contrast with lower v (0.0346 ± 0.00028 m ns^{-1}) in the wetter habitat (CMP_2 corresponding to the wet *Sphagnum* lawn and hollow). The difference in measured v between the different CMP locations can be attributed to the spatial variations in the peat porosities, the entrapped biogenic gas content [cf. *Comas et al.*, 2008] and water table depth, with the associated increase in v through the unsaturated zone.

[28] Common offset measurements along the transect are presented in Figure 4b. The depths of the reflections in the common offset measurements are calculated from a two-layer velocity model. The EM wave velocity above the water table was simulated using the CRIM model [see *Comas et al.*, 2004], assuming an unsaturated moisture content of 0.25 [*Hayward and Clymo*, 1982], giving an unsaturated v of 0.11 m ns^{-1}. Beneath the water table, a constant v of 0.0346 m ns^{-1} was assumed, obtained from CMP_2 within the wet *Sphagnum* lawn and hollow where the water table depth was less than 0.05 m from the peat surface. The two-layer velocity model assumed that the water table depth remained at a constant datum along the

length of the transect; that is, the surface microtopography was associated with variations in the depth of the unsaturated zone, ranging from a minimum depth of 0 m within the wet *Sphagnum* hollow to a maximum depth of 0.61 m within the shrubby-lichen hummocks. The unsaturated v and water table depths were used to calculate the necessary topographic correction to align each trace so that the point where the EM wave hits the water table (assumed to be at a constant datum across the transect) occurs at a depth of 0.0 m. Although this topographic correction enables the core data to be aligned with the GPR measurements, the incorporation of the topographic corrections does introduce image artifacts into common offset measurements. Notably, the pattern of reflections below the peat surface does, in part, follow the surface topography, specifically a distance of between 0.0 and 14.0 m along the transect where the surface topography is most pronounced. Such artifacts result primarily from errors in the derived EM velocity within the unsaturated zone.

[29] Assuming a ground wave velocity of 0.354 m ns^{-1}, an antenna frequency of 200 MHz, and an antenna separation of 0.5 m, the ground wave will influence the received signal for up to 20 ns after the received air wave, to a depth of 0.35 m in the GPR profile. Below this zone, the transect is characterized by two distinctly different patterns of reflections. These areas are identified within Figure 4c as a zone of moderately continuous reflections, marked by black bands, and a zone of chaotic reflections, marked by light gray bands. The zone of chaotic reflections correlates closely with the location of the *S. rubellum* lawn. On the western side of this zone, at a distance of 15 m along the transect, a sharp vertical boundary (the horizontal transition occurs in less than 1 m) exists between the two patterns of reflections. This vertical boundary coincides closely with the transition from the spruce hummock to the *S. rubellum* lawn. On the eastern side, the boundary between the two reflection patterns is sloping. At a distance of 20 m along the transect, the boundary is at a depth of 1.0 m, increasing to a depth of 2.2 m at a distance of 28 m along the transect. This transition zone correlates with the change in the vegetation classification from the *S. rubellum* lawn, through the spruce hummock, to the spruce-tamarack thicket. At the top of the zone of chaotic reflections, the transition from a pattern of semicontinuous reflections to a pattern of chaotic reflections is marked by a horizontal reflector at a depth of approximately 0.9 m, between 19 and 24 m along the transect.

[30] While the pattern of reflections has been broadly classified into two zones above, distinctive variations in the reflection patterns are evident within both the zone of moderately continuous reflections and the zone of chaotic reflections. Within the zone of moderately continuous reflections, the pattern of the reflections differs between the shrubby-lichen hummocks and the spruce-tamarack thicket. The reflections below the shrubby-lichen hummocks are weaker with depth than below the spruce-tamarack thicket. In addition, below the shrubby-lichen hummocks, the reflections are parallel with a small but distinctive easterly dip of approximately 1.5°. In contrast beneath the spruce-tamarack thicket, the reflections are divergent with a westerly dip in the reflections ranging from 0° to 3°. Within the zone of chaotic reflections, the pattern of reflections between 15 and 19 m contrasts with

the pattern of reflections between 19 and 24 m. Between 15 and 19 m, the reflections are more chaotic with a strong variation in the direction and length of the reflections. In comparison, between 19 and 24 m, the reflections are more discontinuous.

3.3. Complex Conductivity Survey

[31] Reciprocal errors were analyzed to identify anomalous measurements (a measurement pair with a larger than expected reciprocal error). Here 254 erroneous independent measurements were identified and discarded from the data analysis. These measurements were discarded because either the maximum measureable voltage of the IRIS Syscal Pro was exceeded or the potential electrode pair included an electrode that was used for current injection immediately prior to its measurement. The latter showed a significant increase in the reciprocal errors ($p < 0.001$). To find a satisfactory parameterization of the FE complex conductivity model (CR2), the data weightings in the least squares objective function, between the remaining measured and simulated resistances (section 2.3), were calculated. These weightings account for variations in measurement and modeling accuracy between the different four-electrode measurement arrays and influence the complexity ("roughness") of the resultant complex conductivity image. Although reciprocal errors of each measurement were obtained, they provide only a single estimate of the error of each data point [*LaBrecque et al.*, 1996]. In addition, reciprocal errors do not account for errors in the FE model (notably, the discretization errors in the FE model and the assumption of a 2-D complex conductivity structure). We therefore simulated the total resistance and chargeability errors to provide a more accurate estimate of the total error. We pooled all estimates of the reciprocal errors, calculated the discretization error in the FE model, and explicitly included an additional error term to account for errors in the FE model. The reciprocal errors of the measured resistances were low, with an average percentage error of 0.14%. The total simulated resistance error was thus low and was assumed to be 0.9%. However, the total resistance error showed significant variation between measurements, ranging from 0.2 to 6.9%. The average reciprocal chargeability error was 4.1%, and the total simulated error was 5.4%.

[32] The real and imaginary conductivity transects are presented in Figure 5 (data are presented on a log scale). The real and imaginary conductivities vary spatially, both horizontally and vertically. The real conductivity ranges from 10 to 120 μS cm^{-1}, and the imaginary conductivity ranges from 0.032 to 0.5 μS cm^{-1}. In the real conductivity image, four regions are clearly identifiable (Figure 5b). Region 1 is a low-conductivity area above the datum (0.0 m, Figure 5), between 0 and 15 m and between 28 and 35 m along the transect. This low-conductivity zone represents the unsaturated zone (datum denotes the water table position). Region 2 is a zone of high-conductivity peat at a depth of 0.0 to 0.6 m below the datum, delineated between 0 and 15 m along the transect. There is evidence of this zone continuing beyond 15 m but with a lower conductivity than is evident between 0 and 15 m. Region 3 is a zone of low conductivity at a depth of 0.6 to 2.5 m below the datum and occurred at a distance of 17–34 m
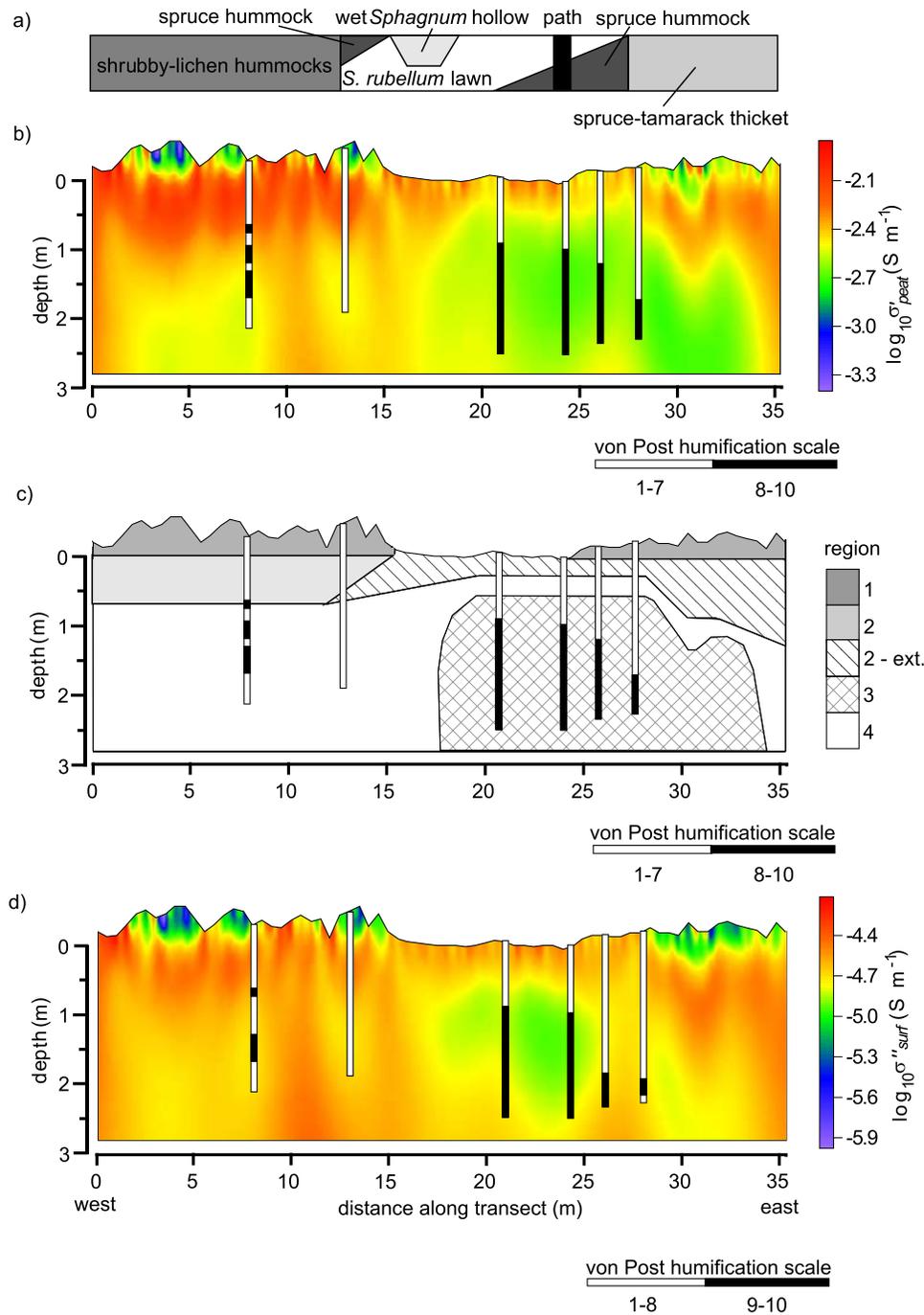
Figure 5. (a) Vegetation types along the west to east study transect. (b) Transect of $\log_{10} \sigma'$ and (c) interpretation of $\log_{10} \sigma'$ transect into regions of varying conductivities. (d) Transect of $\log_{10} \sigma''$. Figures 5b, 5c, and 5d each incorporate the von Post classification of the peat from the six cores. Note the different von Post scale of Figure 5d as opposed to Figures 5b and 5c.

along the transect. Region 4 represents the remainder of the transect, composed primarily of the zone beneath region 2, between 0 and 17 m along the transect. The conductivity of region 4 is between that of the high- and low-conductivity zones, regions 2 and 3, respectively. The imaginary and real conductivities are correlated ($R^2 = 0.61$ and $p < 0.001$). The four regions identified above are, therefore, also evident within the imaginary conductivity image (Figure 5d). However, region 3 in the imaginary conductivity image is more

concentrated between 17 and 25 m and does not extend up to 35 m, as is evident in the real conductivity image.

4. Discussion

[33] The GPR and complex conductivity images show strong spatial variations across the short transect analyzed in this study. These spatial variations correspond with changes in the surface vegetation associated with the different

microhabitats. We present a brief explanation of what may be the dominant factors influencing this spatial variability in the EM reflections and complex conductivity and identify how these spatial variations relate to the different peat properties as revealed by the stratigraphic survey. Finally, we identify how information from the GPR and complex conductivity and stratigraphic surveys combines to give us clues to the developmental history of this part of Caribou Bog.

4.1. Ground-Penetrating Radar

[34] GPR reflections occur where there is a boundary between two zones of differing dielectric permittivities. Within the peat, and below the water table, changes in the dielectric permittivity occur primarily because of changes in the volumetric water content which are caused by changes in the porosity of the peat or its biogenic gas content. Both of these attributes are likely to correlate with the changes in peat type identified within the stratigraphic survey. However, a direct comparison between the GPR and stratigraphic surveys proved problematic. While reflections in the GPR survey correlate with boundaries between different peat horizons, reflections are also evident where no boundaries were identified (Figure 4b). The poor correlation been the GPR and the stratigraphic survey may in part result from the low resolution of the GPR measurements when compared to the dimensions of the identified peat horizons. The vertical resolution of the GPR approach is often assumed to be equal to one quarter to one half of the wavelength [*Sheriff and Geldart*, 1982]. The peak frequency of the received signal from the 200 MHz antenna was 115 MHz, giving a vertical resolution of $0.08-0.16$ m (assuming a velocity of 0.0354 m ns^{-1}) during the common offset measurement survey. With peat horizons as thin as 0.05 m evident in the stratigraphic survey (e.g., C3, $1.32-1.37$ m), the identification of each horizon from the common offset measurements is unfeasible. In addition, in the horizontal plane, the length of the radar reflection footprint parallel to the transect, F_{par}, is equal to [*Sensors and Software*, 1998]

$$F_{par} = \frac{\lambda}{2} + \frac{2d}{\sqrt{K-1}}, \qquad (6)$$

where λ is the peak wavelength, d is the depth, and K is the dielectric permittivity. The length of the radar reflection foot print perpendicular to the transect, F_{perp}, is equal to $F_{par}/2$. Assuming a dielectric constant of 71 (calculated from the GPR wave velocity of 0.0354 m ns^{-1}), at a depth of 1.5 m, F_{par} and F_{perp} equal 0.39 and 0.20 m, respectively. Although the EM reflections identified within the common offset survey vary substantially in length, many are less than 1 m (Figure 4b). This complex 3-D pattern of small reflections, relative to the size of the radar reflection footprint, will further prevent individual peat horizons from being extracted with any confidence. The comparison of the GPR and stratigraphic surveys, therefore, focuses on patterns in the EM reflections and how these correlate with the stratigraphic data. The resolution of the GPR measurements should be borne in mind in the subsequent discussions.

[35] The complicated pattern of layering in C1, C2, C5, and C6 correlate strongly with the zones of moderately continuous reflections identified within the GPR survey. The correlation between the pattern of reflections and the horizons identified within the stratigraphic survey suggests, as postulated above, that the changes in the humification of the peat produce changes in the dielectric permittivity and, thus, EM wave reflections. At a distance of 21 and 24 m along the transect, the strong boundary between the poorly decomposed peat (von Post scores of $3-6$) and the zone of strongly humified peat (von Post scores of 8, 9, and 10) is marked by a strong linear reflection, and the zone of strongly humified peat below coincides with the zone of discontinuous reflections. The zone of chaotic reflections between 15 and 19 m could not be sampled in the stratigraphic survey because of the unstable nature of the surface; the hollow lacked a thick, stable mat of *Sphagnum*. Therefore, no direct evaluation of any change in peat structure is available.

[36] In comparison to the traditional stratigraphic methods applied within this study, the GPR approach provides less detailed information about the structures of the peat. However, the stratigraphic survey is labor intensive and is only able to provide point measurements of the peat profile. In comparison, GPR provides valuable information about the spatial extent of any structural variations. For example, from the GPR survey it can be seen that the patterns of reflections, and thus peat structure, coincide closely with the different habitats. The area characterized by chaotic reflections is evident beneath the entire length of the *Sphagnum* hollow. The pattern of parallel reflections between 0 and 15 extends beneath the entire length of the shrubby-lichen hummocks, and the pattern of westerly dipping reflections extends along the length of the spruce-tamarack thicket. In addition, the zone of well-decomposed peat, identified within C3 and C4, extends across the entire length of the *Sphagnum* lawn.

4.2. Complex Conductivity Survey

[37] If the structural attributes of the peat significantly influence the complex conductivity, spatial variations in σ' and/or σ'' should correlate with the decomposition of the peat identified within the stratigraphic survey. The stratigraphic survey identified a zone of strongly humified peat beneath the *S. rubellum* lawn (von Post humification scale $8-10$). This zone of well-decomposed peat appears to correspond with the area of low σ' (region 3, Figure 5b). In addition, region 2, and its extension (Figure 5c), is characterized by less decomposed peat, and region 4 is characterized by a zone showing distinct layers of peat. The σ'' shows a similar correspondence with the stratigraphic survey because σ'' and σ' are correlated (R^2 = 0.61, section 3.3). The only notable difference is that the low σ'' zone does not extend as far along the transect as the low σ' zone (σ'' increases at a distance of 26 m). The zone of low σ'' therefore correlates with the area of strongly decomposed peat (von Post scores of $9-10$; Figure 5d). Although further stratigraphic data are required to verify the link between the peat decomposition and the complex conductivity, the measurements suggest that structural variations may be identifiable from either σ' or σ''. However, the cause of the spatial variation in σ' and σ'', and therefore the cause of any link with peat decomposition, is unclear. It
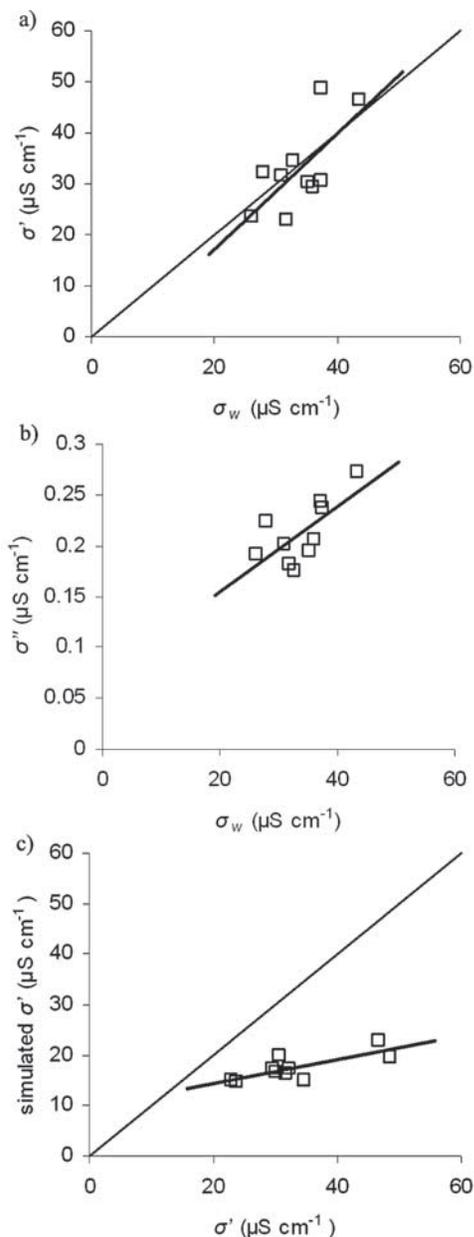
Figure 6. Comparisons of (a) σ' and σ_w, (b) σ'' and σ_w, and (c) simulated σ' and σ'. Thick line shows linear regression; thin line marks 1:1 relationship.

is uncertain whether the variation in complex conductivity beneath the water table results from spatial variations in the volumetric moisture content of the peat (either θ_{eff} or S), σ_w, or the structural changes in the peat properties, specifically, the surface area per unit pore volume. The possible influence of each of these peat properties on σ^* are discussed in turn in sections 4.2.2–4.2.4. This discussion focuses on identifying the cause of spatial variations in σ'. Within peat soils, the petrophysical understanding of σ'' is less fully understood than for σ', and the correlation between σ' and σ'' suggests that similar properties are responsible for the spatial variation of each property.

4.2.1 Volumetric Moisture Content

[38] Beneath the water table, σ' may vary because of changes in the peat saturation (because of entrapped biogenic gas bubbles) and peat porosity (equation (2)). Whether these properties make a significant contribution to the spatial variation in σ' is now considered. The analysis below does not identify whether any change in the structure of the peat associated with the change in porosity, for example, an increased pore surface area, affects σ'. The effect of peat structure is considered within section 4.2.3.

[39] If it is assumed that the peat properties are uniform beneath the water table, i.e., that the variation in σ' results only from a change in the saturation, the maximum entrapped gas content necessary to produce the identified variation in σ' can be approximated from equation (2). In accordance with *Slater et al.* [2007], assuming $n = 1.3$ and $\sigma_{el} \gg \sigma_{surf}$:

$$S = \left(\frac{\sigma'_{unsat}}{\sigma'_{sat}} \right)^{1.3}, \qquad (7)$$

where σ'_{sat} and σ'_{unsat} equal the maximum and minimum measured σ', respectively. To account for the measured variation in σ', the saturation of the peat in the low-conductivity zone (region 3) must equal 0.12. This is unrealistically low. Laboratory measurements of the entrapped biogenic gas content suggest a minimum saturation of, for example, 0.87 [*Baird and Waldron*, 2003].

[40] Without an approximation of m (equation (2)), the spatial variation in the peat porosity necessary to produce the identified variation in σ' cannot be identified. However, variations in the peat porosities are of a similar magnitude to changes in the biogenic gas content (minimum porosity of 0.8 [*Boelter*, 1969]). Because changes in the biogenic gas content cannot account for the spatial variations in the reconstructed σ', it appears improbable that variations in the porosity can account for the identified variation in σ'.

[41] Although variations in the volumetric moisture content of the peat, due to changes in either the saturation or porosity, do not appear to account for the spatial variation in σ', the volumetric moisture content of the peat cannot be excluded as a significant source of variability. Without an accurate parameterization of equation (2), or another mixing model, the effect of spatial variations in the volumetric moisture content cannot be accurately quantified. Most notably, the assumption that $\sigma_{el} \gg \sigma_{surf}$ is unlikely for peat soils.

4.2.2. Pore Water Conductivity

[42] Pore water conductivity affects σ' by altering σ_{el} and σ_{surf} (section 1.3.1). If variations in σ_{el}, resulting from changing pore water conductivities, were the dominant cause of spatial variations in σ', σ' and σ_w should be linearly correlated (equation (2); assuming that σ_{surf} is constant). Measured pore water conductivities ranged from 26.2 to 43.5 μS cm^{-1} ($n = 10$) and were significantly correlated with σ' ($p = 0.03$ and $n = 10$; Figure 6a). In addition, the gradient of the relationship is not significantly different from one, and the intercept is not significantly different from zero. However, there is considerable scatter in the relationship between σ_w and σ' ($R^2 = 0.47$). Therefore, variations in σ' may instead result primarily from variations in σ_{surf} and its associated dependence on the pore water

conductivity. Equation (3), parameterized with the measured pore water conductivities and reconstructed values of σ'', predicts that σ_{el} accounts for only 23% ±3 (mean plus or minus standard deviation) of σ' at the study site, i.e., that σ_{surf} is the dominant conduction pathway. The σ'' and σ_w are linearly correlated ($p = 0.03$ and $n = 10$; Figure 6b); however, considerable scatter is again evident in the relationship ($R^2 = 0.47$). It therefore appears probable that variations in σ' result from variations in both electrolytic and surface conduction. The dependence of σ_{el} and σ_{surf} on the pore water conductivity has been presented by *Comas and Slater* [2004] (equation (3)). Reconstructed and modeled (equation (3)) σ' were significantly correlated ($p = 0.018$ and $n = 10$) and account for a higher proportion of the variability in the reconstructed σ' ($R^2 = 0.56$) than either σ' or σ'' alone. However, equation (3) provides a poor simulation of absolute values of the reconstructed σ', even though the calibration samples used to parameterize equation (3) were obtained from Caribou Bog [*Comas and Slater*, 2004]. Simulated σ' was on average 54% lower than the reconstructed σ', and the gradient of the relationship was significantly different from 1.0, with the model underestimating the measured variation in σ'. However, *Comas and Slater* [2004] presented only a small number of measurements of σ_{surf} and σ'' at low pore water conductivities. In addition, their measurements were conducted on a limited number of peat types from Caribou Bog. Therefore, the importance of σ_{surf} on σ' and its dependence on σ_w at low pore water conductivities remains unclear.

4.2.3. Structural Changes in the Peat Properties

[43] Measurements suggest that σ_w has an important influence on the spatial variation in σ' (section 4.2.2). However, it appears probable that the pore water conductivity was not the only property that significantly influenced σ'. First, considerable scatter is evident in the relationship between modeled and measured σ'. Second, only a limited number of σ_w measurements were obtained across the transect, and no measurements were taken within the high-conductivity zone (region 2). It is uncertain whether there could be a zone of high pore water conductivity at a depth of 0.3 m, at a distance of 8 m along the transect, three times the pore water conductivity at a depth of 1.6 m. Changes in σ', associated with changing σ_w, may therefore be enhanced by spatial variations in the peat properties. For example, higher surface areas or improved interconnectivity of the electrical double layer within certain peat types may enhance surface conduction. However, to identify whether additional peat properties have a significant influence on σ', further data are required to better quantify the magnitude of scatter in the relationship between σ' and σ_w.

4.2.4. Imaginary Conductivity

[44] The identified variation in σ'' and the correlation between σ' and σ'' can be explained by a spatial variation in either the pore water conductivity or the peat structure. At low pore water conductivities, σ_w alters the charge density within the electrical double layer, increasing σ'' [cf. *Comas and Slater*, 2004], while an increased surface area per unit pore volume has been widely shown, at least in mineral soils, to increase σ'' (section 1.3.2). Therefore, the reconstructed σ'' cannot clarify whether changes in peat properties, and the associated variation in surface conduction, has a significant influence on σ', and it cannot be used as a direct measure of changing peat properties. However, unlike σ', σ'' is a function solely of the interfacial surface and does not directly depend on σ_{el}. Therefore, if changing peat properties do significantly influence the complex conductivity, their influence should be more clearly apparent from the reconstructed σ''. The improved correspondence between σ'' and the stratigraphic survey (notably the zone of humified peat, region 3) does suggest that changes in the peat properties could be having an additional influence on the complex conductivity. In addition, the zone of low σ'' below the lawn is also more consistent with the size and shape of the zone of chaotic GPR reflections (section 3.2), suggesting that σ'' is being controlled more significantly by peat structure. This is most evident on the eastern side of the zone of low σ''. The boundary between the zone of high and low σ'' is more consistent with the boundary between the chaotic and moderately continuous GPR reflections than with the boundary between the low and high σ'. The exact cause of the spatial variation in σ^*, therefore, remains uncertain. However, the measurements suggest that it results primarily because of combined changes in both the pore water conductivity and the peat structure.

4.3. Peatland Development

[45] The stratigraphic survey identified different, apparently unconnected peat profiles with different developmental histories. The GPR and complex conductivity surveys have enabled these stratigraphic measurements to be extrapolated along the length of the transect to produce a fully 2-D image of the peat profile. The switches in peat type evident across the length of the hummocky area and the spruce-tamarack thicket suggest wetter and drier phases and wholesale changes in microhabitat. The peat below the lawn consisted of two basic types: upper poorly decomposed peat underlain by gelatinous, strongly decomposed material, with a sharp boundary between the two. The lower gelatinous peat is likely a pool infill, with the pool becoming overgrown by *Sphagnum* more recently to form a lawn and hollow. Without dating of the peat at various depths below the different microhabitats it is difficult to reconstruct the appearance of the peatland in the past. However, it seems that the area currently occupied by the lawn and hollow was a pool for a considerable period of time (thousands of years) during which the surrounding peatland increased in elevation and underwent numerous switches in microhabitat (shown by the layers in C1, C2, and C6). At the same time organic muds, dy or gyttja [cf. *Rydin and Jeglum*, 2006, p. 78], built up in the base of the pool, consolidating to form gelatinous "peat" (strictly, peat is a sedentary deposit, whereas dy and gyttja are sedimentary deposits [cf. *Rydin and Jeglum*, 2006, p. 78]; however, for simplicity, the gelatinous material at the base of the cores from the lawn has been referred to as peat). Interestingly, the pool appears to have been asymmetric, as reported for bog pools studied elsewhere [cf. *Belyea and Lancaster*, 2002], with a steep or vertical western margin and a sloping eastern margin, the latter allowing *Sphagnum* to colonize as a mat which has built in thickness to give the poorly decomposed near-surface peat. That the geophysical data show clearly the asymmetric form of the pool and the bulk contrasts between the *Sphagnum* mat and the dy or gyttja and between the pool peat profile and the profile of peat in the microhabitats

to the west and east suggests that GPR and complex conductivity surveys have considerable potential for helping us reconstruct peatland developmental history.

5. Conclusion

[46] We sought to determine whether ground-penetrating radar and complex conductivity can be used to map subsurface structures within peat deposits in detail over large areas. These approaches revealed spatial variation in the pattern of EM reflections and the real and imaginary conductivities of the peat along the study transect.

[47] The spatial pattern in the EM reflections correlated strongly with the pattern of peat humification obtained from the stratigraphic survey. For example, the location where C3 was extracted, which was composed of strongly humified peat at depths of 0.95 to 2.5 m, was characterized by a pattern of weak and sporadic reflections. The correlation between the stratigraphic and GPR surveys enabled the spatial extent of the differing peat profiles to be identified. This highlighted a strong correlation between the surface habitat and the peat profile. Notably, the hummocky area and the spruce-tamarack thicket were both underlain by a complicated layered profile with varying degrees of humification, suggesting wholesale changes in the microhabitat during the development of the bog. In comparison, the *Sphagnum* lawn was underlain by two principal peat layers which are consistent with a pool becoming infilled with dy or gyttja and then being overgrown by *Sphagnum*.

[48] The conductivity measurements highlight spatial variations in σ' and σ'' along the transect. Comparison with the stratigraphic survey suggests that the approach may have potential for the mapping of spatial variations in the properties of the peat. However, it is currently unclear how the spatial variations in the geophysical measurements correspond to the physical properties of the peat, although the results suggest that the pore water conductivity and the peat structure are the primary properties affecting the complex conductivity. The future application of the complex conductivity approach within peatland studies, therefore, requires the detailed parameterization of petrophysical relationships so that the exact cause of these spatial patterns can be identified. The spatial variation in σ' and σ'' identified here between the differing peatland habitats should act as a driver for this future development.

[49] Despite these problems, the geophysical methods showed considerable promise in being able to identify subsurface features in the peat deposit, such as the infilled pool, and the multiple layers of contrasting peat types under the drier microhabitats. In addition, the methods allowed the horizontal continuity of such features to be mapped. When used to complement traditional stratigraphic surveys, such information will provide the data which are needed for the testing of peatland development and peatland ecohydrological models.

Notation

A constant, dimensionless.
b constant, dimensionless.
C constant, dimensionless.
d depth, m.

F_{par} horizontal footprint length parallel to transect, m.
F_{perp} horizontal footprint length perpendicular to transect, m.
i $\sqrt{-1}$.
K dielectric permittivity, dimensionless.
m cementation factor, dimensionless.
n saturation exponent, dimensionless.
S saturation, dimensionless.
v EM wave velocity, m ns^{-1}.
θ_{eff} effective porosity, dimensionless.
ϕ phase angle, radians.
λ peak wavelength, m.
σ^* complex conductivity, S cm^{-1}.
σ' real conductivity, S cm^{-1}.
σ'' imaginary conductivity, S cm^{-1}.
σ'_{sat} saturated real conductivity, S cm^{-1}.
σ_{el} electrolytic conduction, S cm^{-1}.
σ_{surf} surface conductivity, S cm^{-1}.
σ'_{unsat} unsaturated real conductivity, S cm^{-1}.
σ_w pore fluid or pore water conductivity, S cm^{-1}.
$|\sigma|$ conductivity magnitude, S cm^{-1}.

References

Anderson, L.E., and H. A. Crum (1981), *Mosses of Eastern North America*, Columbia Univ. Press, New York.

Archie, G. E. (1942), The electrical resistivity log as an aid in determining some reservoir characteristics, *Trans. Am. Inst. Min. Metall. Pet. Eng.*, *164*, 54–62.

Baird, A. J., and S. Waldron (2003), Shallow horizontal groundwater flow in peatlands is reduced by bacteriogenic gas production, *Geophys. Res. Lett.*, *30*(20), 2043, doi:10.1029/2003GL018233.

Barber, K. (1981), *Peat Stratigraphy and Climate Change: A Palaeoecological Test of the Theory of Cyclic Peat Bog Regeneration*, A. A. Balkema, Rotterdam, Netherlands.

Belyea, L. R., and A. J. Baird (2006), Beyond the "limits to peat bog growth": Cross-scale feedback in peatland development, *Ecol. Monogr.*, *76*(3), 299–322, doi:10.1890/0012-9615(2006)076[0299:BTLTPB]2.0.CO;2.

Belyea, L. R., and R. S. Clymo (1998), Do hollows control the rate of peat bog growth?, in *Patterned Mires and Mire Pools: Proceedings of the 1998 International Conference*, edited by V. Standen, J. Tallis, and R. Meade, pp. 55–65, Br. Ecol. Soc., London.

Belyea, L. R., and R. S. Clymo (2001), Feedback control of the rate of peat formation, *Proc. R. Soc. London, Ser. B*, *268*, 1315–1321, doi:10.1098/rspb.2001.1665.

Belyea, L. R., and J. Lancaster (2002), Inferring landscape dynamics of bog pools from scaling relationships and spatial patterns, *J. Ecol.*, *90*, 223–234, doi:10.1046/j.1365-2745.2001.00647.x.

Binley, A., and A. Kemna (2005), Electrical methods, in *Hydrogeophysics*, edited by Y. Rubin and S. S. Hubbard, pp. 129–156, Springer, Dordt, Netherlands.

Boelter, D. H. (1969), Physical properties of peats as related to degree of decomposition, *Soil Sci. Soc. Am. Proc.*, *33*, 606–609.

Börner, F. D., and J. H. Schön (1991), A relation between the quadrature component of electrical conductivity and the specific surface area of sedimentary rocks, *Log Anal.*, *32*, 612–613.

Börner, F. D., J. R. Schopper, and A. Weller (1996), Evaluation of transport and storage properties in the soil and groundwater zone from induced

polarization measurements, *Geophys. Prospect.*, 44, 583–601, doi:10.1111/j.1365-2478.1996.tb00167.x.

Comas, X., and L. Slater (2004), Low-frequency electrical properties of peat, *Water Resour. Res.*, 40, W12414, doi:10.1029/2004WR003534.

Comas, X., L. Slater, and A. Reeve (2004), Geophysical evidence for peat basin morphology and lithologic controls on vegetation observed in a northern peatland, *J. Hydrol. Amsterdam*, 295, 173–184, doi:10.1016/j.jhydrol.2004.03.008.

Comas, X., L. Slater, and A. Reeve (2005), Stratigraphic controls on pool formation in a domed bog inferred from ground penetrating radar (GPR), *J. Hydrol. Amsterdam*, 315, 40–51, doi:10.1016/j.jhydrol.2005.04.020.

Comas, X., L. Slater, and A. Reeve (2008), Seasonal geophysical monitoring of biogenic gasses in a northern peatland: Implications for temporal and spatial variability in free phase gas production rates, *J. Geophys. Res.*, 113(), G01012, doi:10.1029/2007JG000575.

Constable, S. C., R. L. Parker, and C. G. Constable (1987), Occam's inversion: A practical algorithm for generating smooth models from electromagnetic sounding data, *Geophysics*, 52, 289–300, doi:10.1190/1.1442303.

Couwenberg, J., and H. Joosten (2005), Self-organisation in raised bog patterning: The origin of microtope zonation and mesotope diversity, *J. Ecol.*, 93, 1238–1248, doi:10.1111/j.1365-2745.2005.01035.x.

Davis, R. B., and D. S. Anderson (2001), Classification and distribution of freshwater peatlands in Maine, *Northeast. Nat.*, 8, 1–50.

Frolking, S., N. T. Roulet, T. R. Moore, P. J. H. Richard, M. Lavoie, and S. D. Muller (2001), Modeling northern peatland decomposition and peat accumulation, *Ecosystems*, 4, 479–498, doi:10.1007/s10021-001-0105-1.

Hayward, P. M., and R. S. Clymo (1982), Profiles of water content and pore size in Sphagnum and peat, and their relation to peat bog ecology, *Proc. R. Soc. London, Ser. B*, 215, 299–325.

Huisman, J. A., S. S. Hubbard, J. D. Redman, and A. P. Annan (2003), Measuring soil water content with ground penetrating radar: A review, *Vadose Zone J.*, 2, 476–491.

Ingram, H. A. P. (1978), Soil layers in mires: Function and terminology, *J. Soil Sci.*, 29, 224–227, doi:10.1111/j.1365-2389.1978.tb02053.x.

Jol, H. M., and C. S. Bristow (2003), GPR in sediments: Advice on data collection, basic processing and interpretation, a good practice guide, in *GPR in Sediments*, edited by C. S. Bristow and H. M. Jol, *Geol. Soc. Spec. Publ.*, 211, 9–27.

Jol, H. M., and D. G. Smith (1991), Ground penetrating radar of northern lacustrine deltas, *Can. J. Earth Sci.*, 28, 1939–1947.

Kemna, A., A. Binley, and L. Slater (2004), Cross-borehole IP imaging for engineering and environmental applications, *Geophysics*, 69, 97–105, doi:10.1190/1.1649379.

LaBrecque, D. J., M. Miletto, W. Daily, A. Ramirez, and E. Owen (1996), The effects of noise on Occam's inversion of resistivity tomography data, *Geophysics*, 61, 538–548, doi:10.1190/1.1443980.

Lapen, D., B. Moorman, and J. Price (1996), Using ground-penetrating radar to delineate subsurface features along a wetland catena, *Soil Sci. Soc. Am. Proc.*, 60, 923–931.

Lesmes, D. P., and K. M. Frye (2001), Influence of pore fluid chemistry on the complex conductivity and induced-polarization responses of Berea sandstone, *J. Geophys. Res.*, 106, 4079–4090, doi:10.1029/2000JB900392.

Lesmes, D. P., and F. D. Morgan (2001), Dielectric spectroscopy of sedimentary rocks, *J. Geophys. Res.*, 106, 13,329–13,346, doi:10.1029/2000JB900402.

Moore, T. R., J. L. Bubier, and L. Bledzki (2007), Litter decomposition in temperate peatland ecosystems: The effect of substrate and site, *Ecosystems*, 10, 949–963, doi:10.1007/s10021-007-9064-5.

Neal, A. (2004), Ground-penetrating radar and its use in sedimentology: Principles, problems and progress, *Earth Sci. Rev.*, 66, 261–330, doi:10.1016/j.earscirev.2004.01.004.

Nobes, D. C., and B. G. Warner (1991), The characterization of bogs using ground penetrating radar, *Open File Rep. 5778*, Ont. Geol. Surv., Toronto, Ont., Canada.

Rydin, H., and J. K. Jeglum (2006), *The Biology of Peatlands*, Oxford Univ. Press, Oxford, U.K.

Scoggan, H. J. (1978), *The Flora of Canada*, Natl. Mus. of Can., Ottawa.

Sensors and Software (1998), *Ground Penetrating Radar Workshop Notes*, Mississauga, Ontario, Canada.

Sheriff, R. E., and L. P. Geldart (1982), *Exploration Seismology*, vol. 1, *History, Theory and Data Acquisition*, Cambridge Univ. Press, New York.

Slater, L., and A. Binley (2003), Evaluation of permeable reactive barrier (PRB) integrity using electrical imaging methods, *Geophysics*, 68, 911–921, doi:10.1190/1.1581043.

Slater, L., and A. Binley (2006), Synthetic and field-based electrical imaging of a zerovalent iron barrier: Implications for monitoring long-term barrier performance, *Geophysics*, 71, 129–137, doi:10.1190/1.2235931.

Slater, L., and D.R. Glaser (2003), Controls on induced polarization in sandy unconsolidated sediments and application to aquifer characterization, *Geophysics*, 68, 1547–1558, doi:10.1190/1.1620628.

Slater, L., and D. Lesmes (2002), IP interpretation in environmental investigations, *Geophysics*, 67, 77–88, doi:10.1190/1.1451353.

Slater, L., and A. Reeve (2002), Investigating peatland stratigraphy and hydrogeology using integrated electrical geophysics, *Geophysics*, 67, 365–378, doi:10.1190/1.1468597.

Slater, L., X. Comas, D. Ntarlagiannis, and M. R. Moulik (2007), Resistivity-based monitoring of biogenic gases in peat soils, *Water Resour. Res.*, 43, W10430, doi:10.1029/2007WR006090.

Swanson, D. K., and D. F. Grigal (1988), A simulation model of mire patterning, *Oikos*, 53, 309–314, doi:10.2307/3565529.

Theimer, B. D., D. C. Nobes, and B. G. Warner (1994), A study of the geoelectrical properties of peatlands and their influence on ground-penetrating radar surveying, *Geophys. Prospect.*, 42, 179–209, doi:10.1111/j.1365-2478.1994.tb00205.x.

Vanhala, H. (1997), Mapping oil-contaminated sand and till with the spectral induced polarization (SIP) method, *Geophys. Prospect.*, 45, 303–326, doi:10.1046/j.1365-2478.1997.00338.x.

von Post, L., and E. Granlund (1926), Sodra sveriges tortillangar I, *Arsb. Sver. Geol. Unders.*, 335, 1–127.

Warner, B. G., D. C. Nobes, and B. D. Theimer (1990), An application of ground penetrating radar to peat stratigraphy of Ellice Swamp, southwestern Ontario, *Can. J. Earth Sci.*, 27, 932–938.

Worsfold, R. D., S. K. Parashar, and T. Perrot (1986), Depth profiling of peat deposits with impulse radar, *Can. Geotech. J.*, 23, 142–154.

———————

A. Baird, Department of Geography, Queen Mary, University of London, Mile End Road, London E1 4NS, UK.

A. Binley and N. Kettridge, Lancaster Environment Centre, Lancaster University, Lancaster LA1 4YQ, UK. (n.kettridge@lancaster.ac.uk)

X. Comas, Department of Geosciences, Florida Atlantic University, Room 360, 777 Glades Road, Boca Raton, FL 33431, USA.

H. Jol, Department of Geography and Anthropology, University of Wisconsin-Eau Claire, 105 Garfield Avenue, P.O. Box 4004, Eau Claire, WI 54702-4004, USA.

L. Slater, Department of Earth and Environmental Sciences, Rutgers University, 101 Warren Street, Smith Hall, Newark, NJ 07102, USA.

M. Strack, Department of Geography, University of Calgary, Calgary, AB T2N 1N4, Canada.

D. Thompson, School of Geography and Earth Sciences, McMaster University, 1280 Main Street West, Hamilton, ON L8S 4K1, Canada.